

7,8-Dichloro-1-oxo- β -carbolines as a Versatile Scaffold for the Development of Potent and Selective Kinase Inhibitors with Unusual Binding Modes[†]

Kilian Huber,[‡] Laurent Brault,[§] Oleg Fedorov,^{||} Christelle Gasser,[§] Panagis Filippakopoulos,^{||} Alex N. Bullock,^{||} Dorian Fabbro,[⊥] Jörg Trappe,[⊥] Jürg Schwaller,[§] Stefan Knapp,^{||} and Franz Bracher^{*,‡}

[‡]Department of Pharmacy, Center for Drug Research, Ludwig-Maximilians University of Munich, Butenandtstrasse 5-13, 81377 Munich, Germany

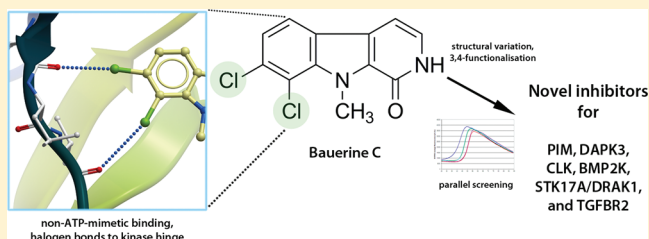
[§]Department of Biomedicine, University Hospital of Basel, Hebelstrasse 20, 4031 Basel, Switzerland

^{||}Nuffield Department of Clinical Medicine, Structural Genomics Consortium, University of Oxford, Old Road Campus Research Building, Roosevelt Drive, Oxford OX3 7DQ, U.K.

[⊥]Novartis Pharma AG, Klybeckstrasse 141, CH-4002 Basel, Switzerland

S Supporting Information

ABSTRACT: Development of both potent and selective kinase inhibitors is a challenging task in modern drug discovery. The innate promiscuity of kinase inhibitors largely results from ATP-mimetic binding to the kinase hinge region. We present a novel class of substituted 7,8-dichloro-1-oxo- β -carbolines based on the distinct structural features of the alkaloid bauerine C whose kinase inhibitory activity does not rely on canonical ATP-mimetic hinge interactions. Intriguingly, cocrystal structures revealed an unexpected inverted binding mode and the presence of halogen bonds with kinase backbone residues. The compounds exhibit excellent selectivity over a comprehensive panel of human protein kinases while inhibiting selected kinases such as the oncogenic PIM1 at low nanomolar concentrations. Together, our biochemical and structural data suggest that this scaffold may serve as a valuable template for the design and development of specific inhibitors of various kinases including the PIM family of kinases, CLKs, DAPK3 (ZIPK), BMP2K (BIKE), and others.



INTRODUCTION

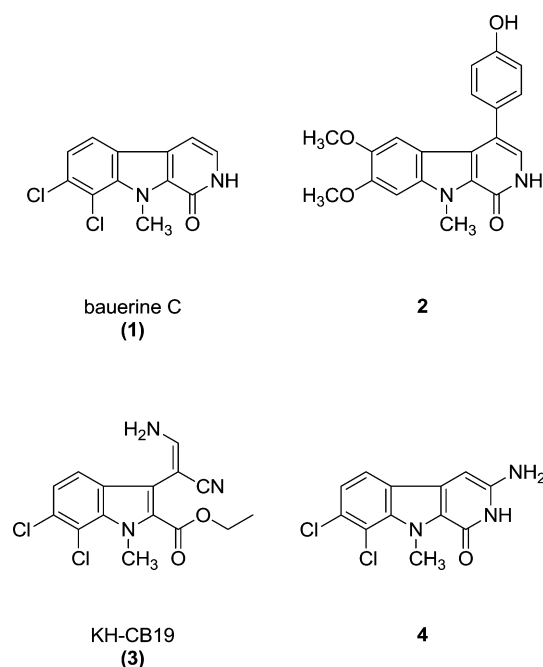
Major drug discovery efforts for novel targeted therapies of various human malignancies focus on the human kinome. This is not surprising because protein kinases, being the largest family of enzymes in mammals,¹ play pivotal roles in many cellular processes including proliferation, differentiation, maintenance, apoptosis, and human disease. Indeed, modulation of phosphorylation signaling pathways by small molecules has demonstrated considerable clinical efficacy in the treatment of devastating disorders such as cancer. The introduction of imatinib² for the therapy of chronic myelogenous leukemia (CML) and more recently the use of crizotinib in anaplastic lymphoma kinase (ALK) dependent tumors³ constitute milestones in the development of modern therapeutics. However, as most kinase inhibitors compete with ATP for binding to highly conserved residues in the enzyme's active site, achieving potent inhibition while preserving selectivity is an issue that substantially contributes to unwanted side effects and thus high failure rates in drug development programs. Consequently, non-ATP-mimetic kinase inhibitors that are anchored to more diverse regions of the ATP binding site may result in more selective inhibitors.

As natural compounds provide a rich source of bioactive chemical scaffolds, we recently investigated the total syntheses of the β -carboline alkaloids bauerines A, B, and C.⁴ Bauerine C (1, Chart 1), isolated from the blue-green alga *Dichotrix baueriana*, features a distinct 6,7-dichloroindole substructure and has been shown to exhibit both antiproliferative and antiviral properties.⁵ In addition, related 1-oxo- β -carbolines such as 2 (Chart 1) have been reported as RET kinase inhibitors⁶ and it has been suggested those compounds are able to interact with hinge backbone residues in a canonical way via the pyridone NH and carbonyl, respectively. Recently, we reported a novel cdc2-like-kinase (CLK) inhibitor, KH-CB19 (3),⁷ which we designed based on the peculiar 6,7-dichloroindole motif of natural compound 1 (Chart 1). Because of methylation at the indole nitrogen, 3 is unable to establish classical hydrogen bond interactions with the hinge backbone. Instead, cocrystal structures of 3 with CLK3 revealed an unusual, non-ATP mimetic binding mode. Selectivity screening against a comprehensive panel of kinases showed that the inhibitor is highly specific for CLK kinases, allowing pharmacologic modulation of alternative

Received: September 27, 2011

Published: December 5, 2011

Chart 1. Bauerine C (1), 1-Oxo- β -carboline RET Inhibitor (2), CLK Inhibitor (3), and 3-Aminobauerine C (4)



pre-mRNA splicing. Notably, we found that compound 3 forms an unusual halogen bond between the 6-chloro substituent and kinase hinge residues. Although those interactions are considered weak in comparison to classical hydrogen bonds, they benefit from a lower desolvation penalty and may very well contribute to inhibitor specificity.⁸ Other well-known examples of carbonyl-halogen interactions include 4,5,6,7-tetrabromobenzimidazole-based inhibitors of CK2.⁹ Our observations with our novel inhibitor 3 prompted us to further explore the chemical and biological space around this scaffold, focusing on diversely functionalized derivatives of alkaloid 1, e.g., 3-aminobauerine C (4) (Chart 1),¹⁰ and in particular substitution patterns that will not allow canonical ATP-mimetic hydrogen bonds with the kinase hinge backbone. We hypothesized that derivatives of 1 either bearing bulky substituents at position 3 or genuine tetracyclic spiro analogues will most likely prevent the classical ATP-mimetic binding mode mediated by the pyridone NH and carbonyl group. In the course of these efforts we incidentally discovered a novel synthetic procedure for the preparation of 3-substituted 4-cyano-1,2,3,4-tetrahydro-1-oxo- β -carbolines.¹⁰ Starting from substituted ethyl 3-cyanomethylindole-2-carboxylates, this approach allows for the convenient synthesis of highly substituted tricyclic (5–8) and tetracyclic spiro (9–11)

analogues of bauerine C (1) as depicted in Table 1. To enable an in-depth investigation of SAR, we expanded our initial set of compounds with a variety of structurally modified analogues 16–24.

Herein, we present the activity of this novel class of compounds as potent and specific inhibitors of a number of serine/threonine kinases including the disease-related kinases PIM1¹¹ and DAPK3. DAPK3, also known as ZIP kinase (ZIPK) or DAP-like kinase (Dlk), belongs to a family of kinases that are part of the CAMK group and that have been implicated in modulation of cell death signaling cascades.¹² Furthermore, it has been shown that DAPK3 is involved in inflammatory processes¹³ and smooth muscle myosin phosphorylation, which suggests DAPK3 as an attractive target for related disorders such as hypertension and asthma.¹⁴ Cocrystal structures of optimized compounds with PIM1 and DAPK3 (ZIPK) revealed an ATP-competitive but not ATP-mimetic binding mode that lacks classical hydrogen bond interactions with the kinase hinge backbone. Instead the chlorine atoms are oriented toward the hinge region and, similar to our CLK inhibitor 3, form in some cases halogen bonds with backbone carbonyls. Because of their distinct binding modes, the screened inhibitors showed a limited number of cross reactivities with other kinases over a comprehensive kinase selectivity panel. Furthermore, selected compounds display interesting differential kinase affinities, indicating that this scaffold may represent a versatile design template for the development of novel BMP2K (BIKE), CLK, and DRAK1 inhibitors which might find clinical applications outside the oncology target area.

RESULTS AND DISCUSSION

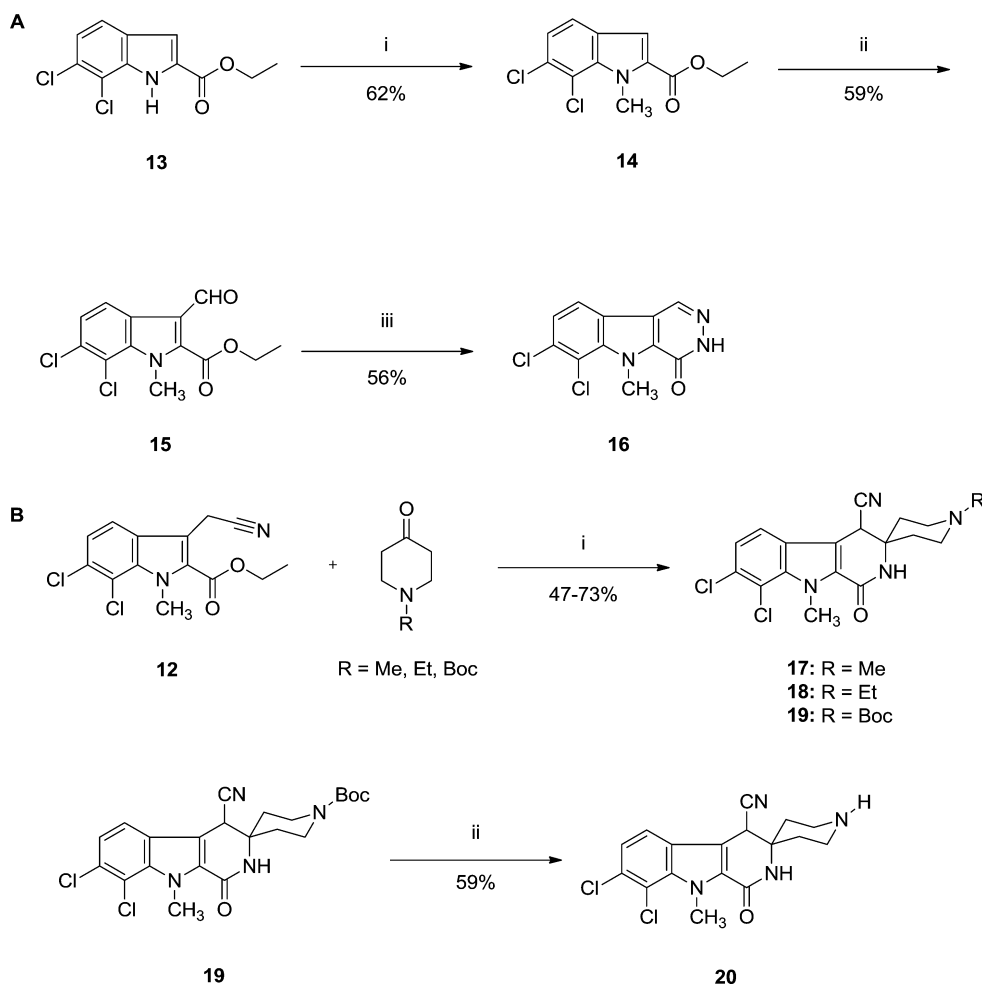
Chemistry. Alkaloid 1 was prepared starting from diazotated 2,3-dichloroaniline and 3-(ethoxycarbonyl)piperidone using a Japp–Klingemann reaction as the crucial step as described in ref 4. The initial set of 1-oxo- β -carbolines including 4 and compounds 5–11 (Table 1) was synthesized by reaction of substituted ethyl 3-cyanomethyl-1H-indole-2-carboxylates such as 12 with gaseous ammonia/ammonium chloride and the corresponding ketones following our previously reported procedure.¹⁰ On the basis of our hypothesis discussed above, four sections of the core scaffold were selected for further modifications in order to establish SAR: (i) the pyridone ring of natural compound 1, (ii) the spirocycle attached to position 3, (iii) the 9-methyl substituent at the indole nitrogen, and (iv) the nitrile group at position 4.

For the preparation of 3-azabauerine C (16) in which the pyridone ring of alkaloid 1 is replaced by a pyridazinone, ethyl

Table 1. Initial Set of 1-Oxo- β -carbolines

Chemical structures of 1-oxo- β -carbolines 5–8 and 9–11 are shown. Structures 5–8 are tricyclic derivatives with substituents R₁, R₂, and R₃ at positions 6, 7, and 9, respectively, and a nitrile group at position 4. Structures 9–11 are tetracyclic spiro derivatives with a chlorine atom at position 6, a methyl group at position 9, and a nitrile group at position 4, and a spirocyclic group at position 3 with substituents R and X.

compd	R ₁	R ₂	R ₃	compd	R	X	n
5	Cl	CH ₃	CH ₃	9	CH ₃	CH ₂	2
6	Cl	H	CH ₃	10	CH ₃	CH ₂	1
7	Cl	CH ₃	CH ₂ CH ₃	11	CH ₃	O	2
8	H	CH ₃	CH ₃				

Scheme 1. (A) Synthesis of 3-Azabauerine C (16)^a and (B) Synthesis of Spiropiperidines 17–20^b

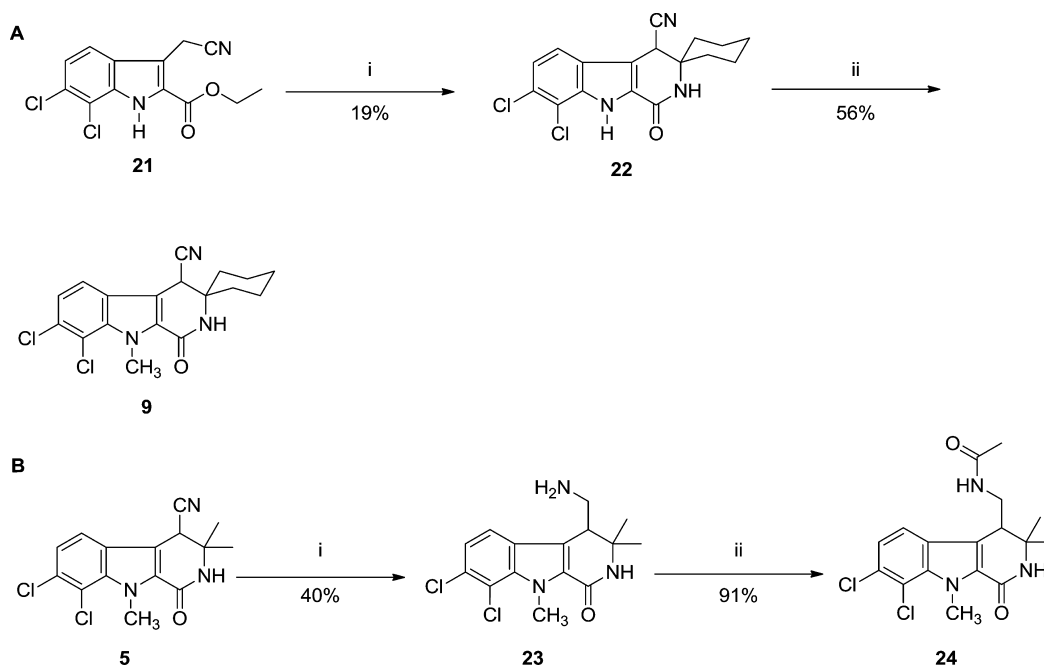
^aReagents and conditions for part A: (i) NaH, DMF, 40 °C, 1 h, then CH₃I, room temp, 5 h; (ii) POCl₃, DMF, room temp, 40 min, then 60 °C, 4 h; (iii) hydrazine, 1,4-dioxane, reflux, 3 h. Percentages given correspond to relative yields. ^bReagents and conditions for part B: (i) NH₃, NH₄Cl, 100 °C, 1 h, sealed tube; (ii) TFA, CH₂Cl₂, room temp, 35 min. Percentages given correspond to relative yields.

6,7-dichloroindole-2-carboxylate (13)¹⁰ was alkylated with methyl iodide in DMF after deprotonation with sodium hydride to give N-methylated indole 14 (Scheme 1A). Formylation of 14 using Vilsmeier conditions afforded carbaldehyde 15 which was cyclized with hydrazine, yielding 3-azabauerine C (16).

To elucidate the effect of heteroatoms within the saturated spiro ring at C-3 of the β -carboline core, nitrogen-containing N-methyl- and N-ethyl-spiropiperidine derivatives 17 and 18 were prepared in the known manner¹⁰ using 12 and appropriate N-alkyl-4-piperidone building blocks (Scheme 1B). Synthesis of N-unsubstituted analogue 20 was achieved via the N-Boc-protected intermediate 19 by cyclization of 12 with N-Boc-4-piperidone, followed by mild deprotection with TFA in dichloromethane.¹⁵ We decided to use the N-Boc-protected intermediate, as the Boc group should be stable toward the strong basic conditions applied during the cyclization step. Furthermore the intermediate was considered to be of possible interest for SAR because of the bulky substituent at the piperidine nitrogen. In order to address the importance of the 9-methyl substituent in the tetracyclic spiro series, 22 was prepared from 21 and cyclohexanone using our general procedure (Scheme 2A). By employment of triethylbenzylammonium chloride (TEBAC) mediated phase-transfer catalysis,¹⁶ 22 can be alkylated with dimethyl sulfate and potassium carbonate in acetonitrile, yielding 9-methyl derivative 9. This protocol allows

for the selective alkylation of the indole nitrogen without affecting the lactam nitrogen and constitutes a feasible alternative to our previously reported procedure for selective N-methylation of 1-oxo- β -carbolines.⁴ To determine the importance of the cyano group at position 4, we chose to prepare primary amine 23 from our original lead compound 5. The reduction of nitriles in the presence of amides is usually quite challenging, since both carbon atoms are at the same oxidation level. Furthermore, in the case of 5, catalytic hydrogenation using Raney nickel, palladium, or platinum on carbon catalysts is not promising because these methods bear the risk of removing halogen substituents from aromatic rings.¹⁷ Initial attempts using sodium borohydride in combination with cobalt or nickel salts¹⁸ were unsuccessful, yet we were able to selectively reduce the cyano group of 5 with tetra-N-butylammonium borohydride (Scheme 2B).¹⁹ Finally, amine 23 was acetylated with acetic anhydride in toluene to give acetamide 24.

Selectivity of 7,8-Dichloro-1-oxo- β -carbolines. All compounds including alkaloid 1 were screened against a kinase panel using a thermal stability shift assay.²⁰ This assay depicts a fast and reliable method to determine a ligand affinity ranking, and the obtained results correlate well with previously published kinetic data.^{7,20} Kinase target hits for active compounds are summarized in Table 2, applying a T_m shift value of 4.0 °C as cutoff (for complete T_m shift screening results, see Table S1 in Supporting

Scheme 2. (A) Preparation of 9-Methyl Analogue 9 via Selective N-Alkylation of 22^a and (B) Synthesis of Primary Amine 23 and Acetamide 24^b

^aReagents and conditions for part A: (i) cyclohexanone, NH_3 , NH_4Cl , 100°C , 1 h, sealed tube; (ii) TEBAC, K_2CO_3 , CH_3CN , room temp, 15 min, then 22 and $(\text{CH}_3\text{O})_2\text{SO}_2$, room temp, 12 h. Percentages given correspond to relative yields. ^bReagents and conditions for part B: (i) Bu_4NBH_4 , CH_2Cl_2 , reflux, 24 h; (ii) Ac_2O , toluene, 80°C , 1 h. Percentages given correspond to relative yields.

Information). Comparison of hits identified in the screen with the kinome tree revealed a distinct and specific pattern of kinase targets (Figure 1). Overall we found that compounds bearing a spiro-piperidine moiety such as 17, 18, and 20 are highly potent inhibitors of PIM1/3 and DAPK3, whereas bauerine C (1) and derivatives 4 and 16 as well as primary amine 23 exhibited exciting activities against so far largely unexplored kinases such as BMP2K and DRAK1.

From investigation of the SAR around parent compound 1 a bit more closely and with particular regard to PIM kinases, the T_m shift assay revealed 3,3-dimethyl derivative 5 and 3-aminobauerine C (4) to exert reasonable affinity toward PIM1, both superior to bauerine C (1) (Table S1, Supporting Information). Notably, compound 6, which does not have a methyl substituent at the indole nitrogen, and the halogen-free analogue 8 showed significantly reduced activity against PIM1 in comparison to 5, suggesting beneficial effects of both the 9-methyl and 7,8-dichloro substituents. Prolongation of alkyl chains at position 3 as in 7 also led to weaker binding, whereas among the initial group of spiro compounds 9, 10, and 11, expansion of ring size and introduction of heteroatoms to the saturated spirocarbocycle seemed to favor activity. Remarkably, removal of the 9-methyl group in the spirocyclohexyl series as in 22 compared to 9 did not result in such a dramatic loss in activity as observed for the tricyclic compounds (5 vs 6), probably indicating a different mode of binding. Reduction of the nitrile group at C-4 again led to a slight decrease in affinity for primary amine 23 in comparison to lead compound 5 with regard to PIM1. N-Acylation of amine 23 to give acetamide 24 resulted in complete loss of activity. Strikingly, investigation of the newly prepared spiro-piperidine compounds revealed 17, 18, and 20 as highly potent inhibitors of PIM1 kinase. The top compound in this series was found to be 20, which is not

substituted at the spiro-piperidine nitrogen. Introduction of an N-methyl substituent as in 17 was well-tolerated; however, an N-ethyl group as in 18 resulted in marginally diminished activity. Notably, N-Boc-protected intermediate 19 did not exhibit any inhibitory potency.

To further examine the selectivity of the newly identified inhibitors, kinase profiling using the thermal shift assay was extended for up to more than 100 kinases (Table S1, Supporting Information). For 20, we observed temperature shifts of $>8^\circ\text{C}$ only for PIM1, PIM3, and DAPK3, emphasizing that compound 20 not only is a highly potent inhibitor of the PIM family of kinases but also displays good selectivity. Among the PIM kinase family, T_m shift data showed a significant lower T_m shift for PIM2, suggesting lower activity of 20 on this target. Similar selectivity patterns were detected for N-methyl- and N-ethylspiro-piperidine derivatives 17 and 18, yet these were slightly less potent against all three PIM kinases and inhibition of DAPK3 was significantly reduced. In general, both tri- and tetracyclic compounds exhibited a comparable trend in activity for PIM1 and CLK1, yet the spiro-piperidines 17, 18, and 20 did give considerably higher T_m shift values for PIM1 compared to CLK1. Among the other compounds, especially 5 and 3-aminobauerine C (4) demonstrated reasonable activity against PIM1.

Interestingly, only parent alkaloid 1 and its closely related derivatives 4 and 16 as well as 5 inhibited TGF β receptor kinase (TGFBR2) with good potency. We also observed moderate activity for 1, 4, and 5 against DRAK1, whereas 3-azabauerine C (16) seems to be quite selective for TGFBR2. However, the most potent compound with regard to DRAK1 was found to be primary amine 23. It is noteworthy that among all evaluated compounds only bauerine C (1) gave a T_m shift of $>8^\circ\text{C}$ for BMP2K.

Table 2. Kinase Targets with $\Delta T_m > 4\text{ }^\circ\text{C}$ ^a

compound	1	4	5	6	7	8	9	10	11	16	17	18	19	20	22	23	24
AAK1	4,6	2	2,2	1,1	1,7	0,6	1,7	1,5	2,6	3,9	0,9	0,2	0,3	1,5	2,4	0,8	0,2
BIKE	8,2	5,2	2,8	1,2	1,2	1,1		1,3	2,3	5,3	0,8	-0,5	0	1	1,1	1,7	0,4
CLK1	4,6	5,9	6,4	5,3	3,5	2,4	4	4,8	4,6	3,9	5,7	4	0,5	7	5,4	5,1	2,6
CLK4	3,2	2,1	4,3	4,9	2,8	1,4	1,1	3,3	2,8	0,9	2,1	1,8	0	4,6	5,7	2,8	1,4
CK2 α 2	2	3	2,1	1,9	1	0,7	0,8	1	1	2,1	2,7	1,8	0,3	4,2	1,2	0,5	1
DAPK3	3,4	2,6	3,4	2	2,4	0,6	4,7	1,5	3,1	4	6,3	4,6	-0,2	10,6	3,4	3,6	0,8
DYRK2	4,1	2,4	2	1,3	0,6	0,5		0,7	1	1,6	1,3	0,9	0,3	3,6	1,4	0,2	0,9
FES	0,1	0,4	-0,3	-0,2	0	0		0	0	0,2	0,5	0,7	0,4	4	-0,4	0,3	0,4
GAK	3,3	4,3	2,8	2,5	1,2	0	0,9	1,2	1,3	1,6	0,8	0,9	-0,2	1,4	2,8	0,7	0,5
Haspin	3,4	2,7	0,9	0,3	0,4	1,7		0,1	1,1	3,2	3,4	2,6	0,3	5,6	0	1,8	0,3
GSK3 β	1,4	2,9	5,6	4,7	2	1,8		2,5	3,4	4,6	2,2	1,5	-0,2	3,9	2,6	0,6	0,2
SgK085	6,4	2,9	2	3,1	0,4	1,7	0,5	0,1	0,5	5,5	1,5	0	0	3,5	1,2	0,2	0,6
PIM1	4	4	5,7	3,5	3,3	0,9	4,7	3,8	4,8	1,6	7,7	7,4	0,8	10,7	4,9	3,6	1,1
PIM2	2,9	3	3,6	2,3	2	-0,2		1,6	2,2	1,6	5,2	3,9	-0,2	6,5	1,4	3,2	0,7
PIM3	3,6	3,6	6,2	4	3,4	1,3	4	3,8	4,7	2,3	7,2	7,1	0,6	9,6	4,9	3,7	0,7
PLK1	1,6	1,4	4,9	4	0,9	3,2		1,3	0,8	3,1	0,6	0,4	0,5	1,4	0,3	-0,6	0,7
PLK4	1,7	2	5,1	1,7	4,6	0,9		2,5	2,7	1,5	3,3	3,2	0,1	6,8	1,3	2,7	1
PKC γ	1,2	0,2	1,7	0,7	0,8	0,4		0,5	1	1,2	3,9	4,5	0,2	6,1	1,3	1,7	0
PRKX	0,3	0,8	2,8	1,2	0,8	0,5		0,7	1,4	0,3	3,3	3,1	0,3	5,8	1	3,3	0,7
RSK1~b	4,6	3,1	1,8	1,4	0,5	0,4		0,5	0,6	1,7	0,5	0	0	1	0,4	0,4	0,7
DRAK1	6,2	6,9	5,8	3	2,6	0,5	3	2	2,7	3,5	2,7	1,6	0,6	4,3	2,2	7,5	0,9
DRAK2	3,6	3	4,8	2,1	2,9	0,3	2,9	2,6	1,7	2,2	1,2	1,1	0	3,4	2,3	6,4	1,6
STK33	2,3	0,4	2,2	1,1	0,6	1		0,2	0,7	1,2	2,2	2,1	0,3	5,9	0,5	0,9	0,3
TGFBR2	10,1	7,9	8,1	6,8	5	2,9		2,2	2,6	10,4	1,1	0,3				3	1,5
RSK4~b	4	1,2	2,3	0,1	-0,1	0,1		0,1	0	1,4	0,2	0,2	-0,4	0,8	-0,2	0,7	0,4

^aSee Table S1 (Supporting Information) for complete thermal shift assay data. Values are shown in $^\circ\text{C}$. Empty spaces indicate that no data have been measured. Targets with significant T_m shift have been colored in red ($>8\text{ }^\circ\text{C}$) and yellow ($>4\text{ }^\circ\text{C}$), respectively.

In order to revalidate the results obtained in the thermal shift assay, we also determined IC_{50} values for our most potent compound **20**. In a kinetic enzyme assay using $100\text{ }\mu\text{M}$ ATP, we determined IC_{50} values of 60 and 90 nM for PIM1 and PIM3, respectively (data not shown). To further corroborate the data obtained in the T_m shift assay, we also screened our top inhibitor **20** against a comprehensive kinase selectivity panel (Table 3). In general, the kinetic data correlated well with the results from the T_m shift assay, although we identified CAMK2 and PKA as additional targets that were inhibited by **20** with IC_{50} values below 100 nM. This may be related to the activation state of these two kinases, since inactive enzymes were used for T_m screening. In summary, the main cross-reactivities of compound **20** are within the AGC family, in particular with PKA, ROCK, and PKN1/2. Outside the AGC family we observed cross-reactivity with CK1 and CaMK2 (Figure 1). However, in contrast to the clinically evaluated imidazo[1,2-*b*]pyridazine-based PIM inhibitor SGI-1776,²¹ compounds **17** and **20** did not exhibit any significant activity against PDGFR α , FLT3, or KIT.

Binding Mode. To gain insights on the binding mode and thus be able to rationalize SAR, we first determined the crystal structures of **17** and **20** in complex with PIM1 (PDB codes 3CXW and 3CY2) (Figure 2A and Supporting Information

Figure S1). The structures revealed that both inhibitors do not establish any classical hydrogen bond interactions with the hinge region. Interestingly, the lactam moiety does not contribute to inhibitor binding, as the hydrophobic dichlorobenzene ring is oriented toward the hinge while the pyridone and spiro-piperidine rings are pointing toward the back of the binding pocket. This allows formation of bidentate H-bonds between the spiro-piperidine nitrogen and Asn172 as well as Asp186. The observed binding mode for **17** and **20** is therefore in contrast to the one described for other 1-oxo- β -carboline reported as CDK2 or RET inhibitors.^{6,22} As shown in Figure 3, compounds that are not substituted at positions 3 and 4 are likely to establish classical, ATP-mimetic interactions between the pyridone ring and kinase hinge backbone residues. These can be mediated via formation of a hydrogen bond between the inhibitor's lactam carbonyl and the backbone NH of Leu83 (CDK2 numbering) and a second one between the pyridone-NH and Glu81 (Figure 3A). Alternatively, all interactions can be established between the pyridone moiety and Leu83 exclusively (Figure 3B). However, either of those binding modes is incompatible with **17** and **20**, probably because of the bulky nature of the spiro ring which prevents the novel inhibitors from assuming an ATP-mimetic orientation.

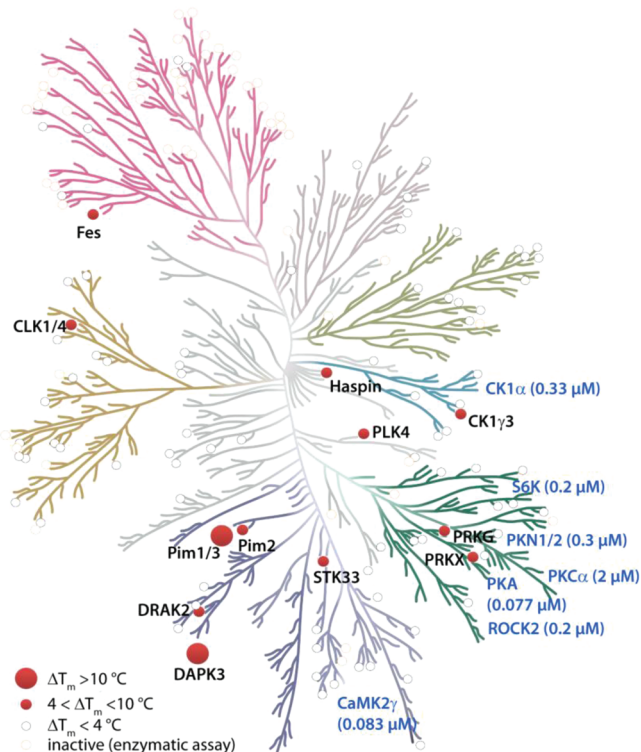


Figure 1. Kinome tree visualization of inhibitor selectivity for compound **20** combining both T_m shift and kinetic assay results (illustration reproduced courtesy of Cell Signaling Technology, Inc. (www.cellsignal.com)).

Table 3. In Vitro Kinase IC_{50} Values Determined for Compound **20**

target	IC_{50} (μM)	target	IC_{50} (μM)	target	IC_{50} (μM)
ALK	>10	HCK	>10	PKB α	>10
AURORA A	>10	HER1	>10	PKC α	2.2
AXL	>10	HER2	>10	PKC θ	1.4
BTKv2	>10	HER4	>10	PKN1	0.31
cABL	>10	IGF1R	>10	PKN2	0.30
cABL _{T315I}	>10	Ins1R	>10	PLK1	>10
CaMK2	0.083	IRAK4	>10	RET	7.7
CDK2	>10	JAK1	>10	ROCK2	0.22
CDK4/D1	>10	JAK2	>10	RON	>10
CK1 α	0.33	JAK3	>10	S6K	0.23
cKIT	>10	KDR	7.2	SYK	>10
cMET	>10	LCK	>10	TYK2	>10
COT1	>10	LYN	>10	VPS34	>9.1
CSK	>10	MK2	>10	WNK1	>10
cSRC	>10	MK5	1.7	YES	>10
EphA4	>10	mTOR	>9.1	ZAP70	>10
EphB4	>10	p38 α	>10	PKA	0.077
ERK2	>10	PAK2	>10	GSK3 β	>10
FAK	>10	PDGFR α	>10	PIM2	0.24
FGFR-1	>10	PDK1v2	>10	FYN	>10
FGFR-2	>10	PI3K α	>9.1	FLT3	>10
FGFR-3	>10	PI3K β	8.6	PI4K β	2.5
FGFR3K	>10	PI3K δ	4.7	PI3K γ	3.1
FGFR-4	>10				

Looking back at our PIM1 complex, we surprisingly found that the cyano group is not involved in a hydrogen bond interaction with Lys67, which is in contrast to comparably substituted 3-cyanopyridones reported as PIM inhibitors by

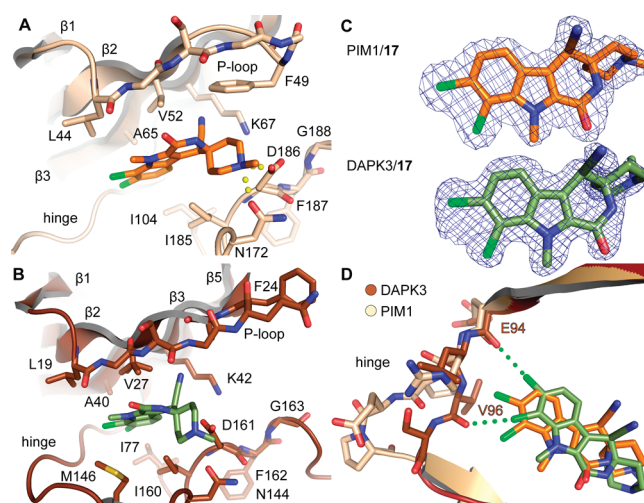


Figure 2. (A) Crystal structure of **17** bound to PIM1 (PDB code 3CXW). Hydrogen bonds are depicted as yellow dots. (B) Cocystal structure of **17** in complex with human DAPK3 (PDB code 3BHY). (C) Comparison of electron density maps of **17** bound to PIM1 (top) or DAPK3 (bottom), respectively. (D) Superimposition of hinge areas of PIM1 and DAPK3 structures with bound inhibitor **17**. Halogen bonds are shown as green dots.

Cheney et al. (PDB code 2OBJ).²³ Various other PIM inhibitor scaffolds, e.g., pyrrolo[2,3-*a*]carbazoles²⁴ and 3*H*-benzo[4,5]-thieno[3,2-*d*]pyrimidin-4-ones,²⁵ also form hydrogen bonds with this highly conserved residue. The DFG motif assumes an active “in” conformation, and two hydrophobic residues, the gatekeeper Leu120 and the DFG-adjacent Ile185, enclose the tricyclic core ring system (not shown). As in several other reported PIM inhibitor complexes,^{20,24,26–28} **17** and **20** also induce a conformational change in the glycine-rich P-loop by which Phe49 flips into the active site (not shown). This structural rearrangement on the one hand enables additional stacking effects with the inhibitor but also shifts the kinase in an inactive conformation which is incompatible with substrate binding. Regarding the difference in activity observed for different PIM isoforms, despite the high sequence homology among all three isoforms, kinetic studies suggest that ATP K_M values for PIM1/PIM3 and PIM2 differ remarkably.²⁹ This may explain the so far unsuccessful efforts to target all three kinases with an ATP-competitive inhibitor. PIM2 has a leucine residue instead of glutamate at position 124 in the hinge region, which disrupts the polar interactions with Arg122 observed in PIM1.³⁰ As a result, the arginine side chain is disordered, which in combination with another amino acid change (Val126Ala) might influence hinge dynamics and hence inhibitor binding due to reduced availability of hydrophobic interactions and higher desolvation energy.²⁵ In PIM3 the glutamate residue at position 124 is conserved but like PIM2 Val126 is replaced by alanine which may cause slightly weaker binding of the inhibitors.

Interestingly, the DAPK3 cocystal structure with **17** (PDB code 3BHY) revealed a different mode of binding compared to the PIM1 structure (Figure 2B). In the DAPK3 complex, the inhibitor’s lactam carbonyl establishes a hydrogen bond with a water molecule in the active site which itself is involved in a hydrogen bond network with Ser21 (not shown). The spiro-piperidine ring appears a little more twisted compared to the PIM1 structure (Figure 2C) and does not seem to participate in any polar interactions. However, the electron density for the piperidine in the obtained cocystal structure

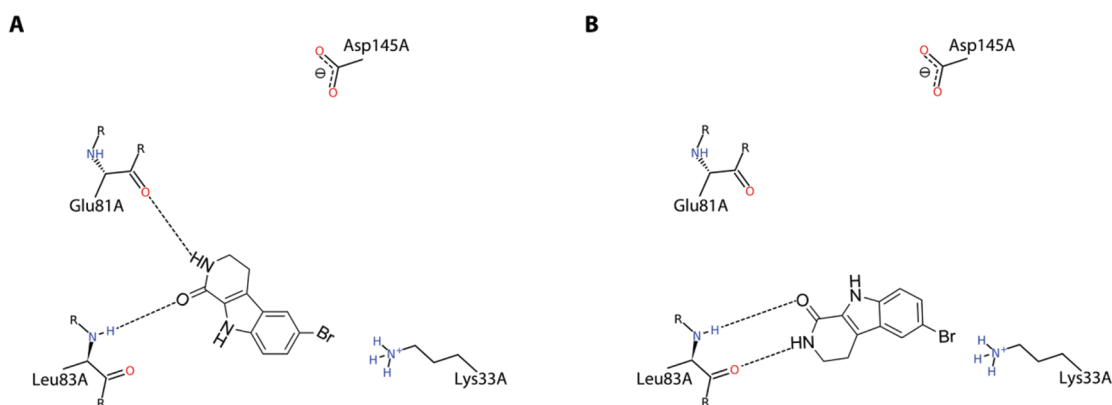


Figure 3. Canonical binding mode of 1,2,3,4-tetrahydro-1-oxo- β -carbolines docked into human CDK2. In contrast to the spirocyclic compound **17** (Figure 2) main interactions are mediated between the inhibitor's lactam ring and kinase hinge backbone residues Glu81 and Leu83 (A) or Leu83 exclusively (B).

was weak, possibly indicating multiple conformations for this moiety. Similar to PIM1, **17** benefits from hydrophobic interactions with the gatekeeper (Leu93) and an isoleucine (Ile160) residue N-frontal to the DFG motif (not shown). More interestingly, in this structure we observed establishment of halogen bonds between the 7,8-dichloro substituents of **17** and the backbone carbonyl of Glu94 and Val96, respectively (Figure 2D), similar to the interactions we had discovered for our recently reported novel CLK inhibitor **3** (PDB code 2VAG).⁷ The expanded nature of the hinge region in PIM1 due to insertion of two proline residues (Pro123 and Pro125) prohibits formation of such a halogen bond as illustrated in Figure 2D.³¹ In the DAPK3 complex the halogen in position 8 was partially radiolyzed. Additional electron density observed in the vicinity of the 7,8-dichloro substituents was interpreted as a chloride ion with partial occupancy. We also observed complete radiolysis of the C–Cl bond at this position in the data set collected on the PIM1 complex with **20** (PDB code 3CY2, Supporting Information Figure S1).

Cellular Assays. As aberrant expression of PIM kinases has been observed for numerous types of cancer, e.g., leukemia,^{32–34} lymphoma,^{35,36} and solid tumors such as prostate,^{37,38} colon,³⁹ and pancreatic⁴⁰ cancer, we evaluated the antiproliferative potential of our most potent inhibitor **20** and its effects on PIM downstream signaling. For this purpose, **20** was screened against five human leukemia cell lines and IC₅₀ values were determined after 48 h of treatment, showing low micromolar potency comparable to data previously reported for imidazo[1,2-*b*]pyridazine PIM inhibitors (Table 4).⁴¹ However, consistent with our observation that **20** is selective for PIM1 with regard to FLT3 in contrast to imidazo[1,2-*b*]pyridazine-based PIM inhibitors, cytotoxic activity for cell lines harboring the FLT3-ITD mutation such as MV4;11 and MOLM13 was reduced. To further confirm the biological activity of our lead compound, we also tested **20** for its ability to inhibit phosphorylation of a known PIM downstream target. Using the human MV4;11 acute myeloid leukemia (AML) cell line, we found a dose-dependent decrease in phosphorylation of 4E-BP1¹¹ as a result of PIM inhibition by **20** (Figure 4).

CONCLUSION

In this study we present substituted 7,8-dichloro-1-oxo- β -carbolines as a novel and versatile scaffold for the development of non-ATP-mimetic kinase inhibitors. SARs around the core scaffold which we derived from the natural compound bauerine

Table 4. Comparison of Cellular IC₅₀ Values Determined for Compound **20 and an Imidazo[1,2-*b*]pyridazine-Based Inhibitor**

cell line	IC ₅₀ (μ M) ^a	
	20	K00135 (imidazo[1,2- <i>b</i>]pyridazine-type inhibitor)
MV4;11 (MLL, FLT3-ITD-positive)	2.07	0.4
RS4;11 (ALL)	3.57	8.8
MOLM13 (AML, FLT3-ITD-positive)	3.25	0.3
SEM (ALL)	4.68	6
K562 (CML, blast crisis)	6.49	8

^aDeterminations were done after 48 h of preincubation. K00135 values are adopted from ref 41.

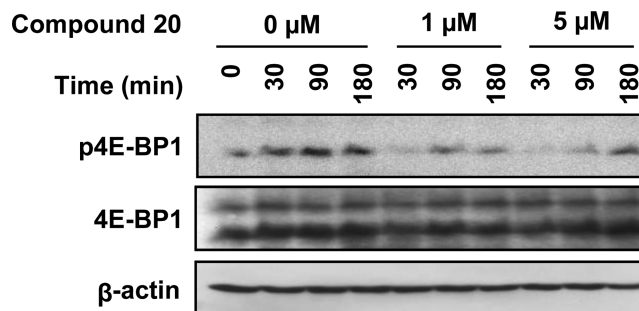


Figure 4. MV4;11 cells were incubated with increasing concentrations of **20** for indicated times and harvested, and protein extracts were separated by SDS–PAGE. The effect of **20** on the PIM endogenous target 4E-BP1 was followed by Western blotting with the indicated phosphospecific antibody. Membranes were stripped and reprobbed with nonphosphospecific and anti-actin antibodies to check for equal loading.

C (1) were established, and optimized compounds of the 4-cyano-1,2,3,4-tetrahydro-1-oxo- β -carboline type such as the spiroperidine **20** are highly potent inhibitors of the oncogenic PIM kinases and DAPK3 (ZIPK). Because of their unusual binding mode revealed by X-ray crystallography, the inhibitors display good specificity among a comprehensive kinase selectivity panel with only a few off-targets within and outside the AGC family. Upon binding to PIM1 the inhibitors induce a

conformational change in the P-loop, which shifts the kinase into an inactive state. The novel compounds also exhibit efficacy in cellular assays, as **20** was found to deplete PIM-dependent phosphorylation of downstream effector proteins and demonstrated antiproliferative activity at low micromolar concentrations in related cell viability screens. Importantly, we found an intriguing binding mode for the *N*-methyl analogue **17** in complex with DAPK3 which revealed formation of halogen bonds with the kinase hinge region. These interactions may contribute to inhibitor selectivity and further underscore the interesting features and versatility of our 6,7-dichloroindole scaffold. Because of active site similarities, this novel class of compounds may also serve well as template for the preparation of new CLK inhibitors.⁷ Moreover, activities observed for some of the other analogues presented herein indicate that selected compounds such as alkaloid **1** and primary amine **23** could also be optimized for the development of new targeted inhibitors of BMP2K (BIKE) and DRAK1. Consequently, efforts to further improve potency and selectivity of those compounds are under way.

EXPERIMENTAL SECTION

General Information. NMR spectra were recorded on a JEOL JNMR-GSX 400 and a JEOL JNMR-GSX 500 (JEOL, Peabody, MA, U.S.), using TMS as internal standard. Chemical shifts are given in ppm, and coupling constants are given in hertz. The spectra were recorded at room temperature, unless stated otherwise. Mass spectra (electronic ionization, EI, 70 eV) were recorded using a Hewlett-Packard 5989 A mass spectrometer with a 59980 B particle beam LC/MS interface (Agilent Technologies, Palo Alto, CA, U.S.). IR spectra were recorded as KBr disks on a Perkin-Elmer FT-IR Paragon 1000 (Perkin-Elmer, Waltham, MA, U.S.) or JASCO FT/IR-410 (JASCO, Easton, MD, U.S.). Melting points were determined with a Büchi B-540 apparatus (Büchi, Flawil, Switzerland) and are uncorrected. Elemental analyses were performed using a CHN-Elementaranalysator Rapid (Heraeus, Hanau, Germany) or Elementaranalysator Vario EL (Elementar, Hanau, Germany). Purification by flash column chromatography (FCC) was done using silica gel 60 (Merck, Darmstadt, Germany). The purity of the synthesized compounds was determined and confirmed by combustion analysis.

All chemicals were purchased from Sigma-Aldrich, Fluka, and Acros and used without further purification.

Bauerine C (**1**) was prepared as reported previously,⁴ and procedures and spectral data for compounds **4–12** and **21** are provided in ref 10. For procedures and experimental data for compounds **14** and **15** as well as general additional spectroscopic data see Supporting Information.

6,7-Dichloro-5-methyl-3H-pyridazino[4,5-*b*]indol-4(5H)-one Hemihydrate (16**).** Compound **15** (474 mg, 1.6 mmol) and hydrazine hydrate (192 mg, 4.8 mmol) were dissolved in 1,4-dioxane (50 mL), and the mixture was heated to reflux for 3 h. After the mixture was cooled, the crude precipitated product was filtered off and recrystallized from ethyl acetate to give 241 mg (56%) of **16** as a yellow solid. Mp 307 °C; ¹H NMR (400 MHz, DMSO-*d*₆) δ 12.96 (br s, 1 H, N–H), 8.78 (s, 1 H, 1-H), 8.19 (d, *J* = 8.5 Hz, 1 H, 9-H), 7.56 (d, *J* = 8.5 Hz, 1 H, 8-H), 4.63 (s, 3 H, N–CH₃); MS EI *m/z* (relative intensity, %) 270 [M⁺ + 4] (14), 268 [M⁺ + 2] (67), 266 [M⁺] (100). Anal. (C₁₁H₇Cl₂N₃O·0.5H₂O) C, H, N.

General Procedure for Preparation of Spiro-4-cyano-1-oxo-β-carbolines. Synthesis of compounds **17–19** and **22** was achieved by using the previously reported procedure.¹⁰ Briefly, the appropriate ethyl 3-(cyanomethyl)indole-2-carboxylate (**12** or **21**, 3.21 mmol) and ammonium chloride (6.42 mmol) were suspended in the given amount of ketone in a glass tube. After the mixture was cooled to –80 °C, gaseous ammonia was introduced into the tube until an amount of ~10 mL was condensed. The tube was closed tightly and heated to 100 °C for 16 h in an autoclave. The mixture was allowed to reach room temperature and after evaporation of excess ammonia extracted with ethyl acetate (3 × 30 mL). The combined organic layers were dried over sodium sulfate,

filtered, and the solvent was removed. The crude product was purified by flash column chromatography.

(4′RS)-7′,8′-Dichloro-1,9′-dimethyl-1′-oxo-1′,2′,4′,9′-tetrahydrospiro[piperidine-4,3′-pyrido[3,4-*b*]indole]-4′-carbonitrile (17**).** **17** was prepared from **12** (1.00 g, 3.21 mmol) and *N*-methyl-4-piperidone (5 mL) following the general procedure for preparation of spiro 4-cyano-1-oxo-β-carbolines. Eluent for FCC was dichloromethane/ethanol (3:1). The crude product was recrystallized from ethanol to give 568 mg (47%) of **17** as pale pink crystals. Mp 284 °C; ¹H NMR (400 MHz, DMSO-*d*₆, 50 °C) δ 8.12 (br s, 1 H, N–H), 7.88 (d, *J* = 8.6 Hz, 1 H, 5′-H), 7.43 (d, *J* = 8.6 Hz, 1 H, 6′-H), 4.97 (s, 1 H, 4′-H), 4.46 (s, 3 H, 9′-CH₃), 2.66 (m, 1 H, 2′-6′-H), 2.47 (m, 1 H, 2′-6′-H), 2.33 (br t, *J* = 5.5 Hz, 2 H, 2′-6′-H), 2.22 (s, 3 H, 1-CH₃), 2.06 (m, 1 H, 3′-5′-H), 1.97 (m, 1 H, 3′-5′-H), 1.70 (br t, *J* = 5.5 Hz, 2 H, 3′-5′-H); MS EI *m/z* (relative intensity, %) 380 [M⁺ + 4] (8), 378 [M⁺ + 2] (35), 376 [M⁺] (53), 317 (100), 236 (30), 195 (23). Anal. (C₁₈H₁₈Cl₂N₄O) C, H, N.

(4′RS)-7′,8′-Dichloro-1-ethyl-9′-methyl-1′-oxo-1′,2′,4′,9′-tetrahydrospiro[piperidine-4,3′-pyrido[3,4-*b*]indole]-4′-carbonitrile (18**).** **18** was prepared from **12** (1.00 g, 3.21 mmol) and *N*-ethyl-4-piperidone (5 mL) following the general procedure for preparation of spiro 4-cyano-1-oxo-β-carbolines. Eluent for FCC was dichloromethane/ethanol (5:1). The crude product was recrystallized from ethanol to give 914 mg (73%) of **18** as white crystals. Mp 276 °C; ¹H NMR (500 MHz, DMSO-*d*₆, 50 °C) δ 8.15 (br s, 1 H, N–H), 7.89 (d, *J* = 8.5 Hz, 1 H, 5′-H), 7.43 (d, *J* = 8.5 Hz, 1 H, 6′-H), 4.97 (s, 1 H, 4′-H), 4.46 (s, 3 H, 9′-CH₃), 2.70 (m, 1 H, 2′-6′-H), 2.48 (m, 1 H, 2′-6′-H), 2.38 (q, *J* = 7.1 Hz, 2 H, CH₂CH₃), 2.36 (br t, *J* = 5.5 Hz, 2 H, 2′-6′-H), 2.05 (m, 1 H, 3′-5′-H), 1.97 (m, 1 H, 3′-5′-H), 1.70 (br t, *J* = 5.5 Hz, 2 H, 3′-5′-H), 1.00 (t, *J* = 7.1 Hz, 3 H, CH₂CH₃); MS EI *m/z* (relative intensity, %) 394 [M⁺ + 4] (8), 392 [M⁺ + 2] (44), 390 [M⁺] (69), 375 (18), 317 (100), 236 (21), 195 (20). Anal. (C₁₉H₂₀Cl₂N₄O) C, H, N.

(4′RS)-tert-Butyl 7′,8′-Dichloro-4′-cyano-9′-methyl-1′-oxo-1′,2′,4′,9′-tetrahydrospiro[piperidine-4,3′-pyrido[3,4-*b*]indole]-1-carboxylate (19**).** **19** was prepared from **12** (1.00 g, 3.21 mmol) and *N*-Boc-4-piperidone (4.50 g, 22.58 mmol) following the general procedure for preparation of spiro-4-cyano-1-oxo-β-carbolines. Eluent for FCC was petroleum ether/ethyl acetate (1:1). The crude product was recrystallized from ethanol to give 722 mg (49%) of **19** as white crystals. Mp 250 °C; ¹H NMR (500 MHz, CDCl₃, 50 °C) δ 7.58 (d, *J* = 8.5 Hz, 1 H, 5′-H), 7.31 (d, *J* = 8.5 Hz, 1 H, 6′-H), 6.28 (br s, 1 H, N–H), 4.55 (s, 3 H, 9′-CH₃), 4.15 (s, 1 H, 4′-H), 3.95 (d, *J* = 14.3 Hz, 1 H, 2′-6′-H), 3.83 (d, *J* = 14.0 Hz, 1 H, 2′-6′-H), 3.32 (dd, *J* = 12.0 Hz, 2.5 Hz, 1 H, 2′-6′-H), 3.23 (dd, *J* = 11.8 Hz, 2.0 Hz, 1 H, 2′-6′-H), 2.15 – 2.02 (m, 2 H, 3′-5′-H), 1.91 (d, *J* = 14.0 Hz, 1 H, 3′-5′-H), 1.81 (dd, *J* = 12.0 Hz, 2.5 Hz, 2 H, 3′-5′-H), 1.47 (s, 9 H, C (CH₃)₃); MS EI *m/z* (relative intensity, %) 466 [M⁺ + 4] (2), 464 [M⁺ + 2] (14), 462 [M⁺] (20), 389 (31), 362 (75), 333 (32), 317 (100), 305 (88), 264 (59), 236 (54), 195 (35). Anal. (C₂₂H₂₄Cl₂N₄O₃) C, H, N.

(4′RS)-7′,8′-Dichloro-9′-methyl-1′-oxo-1′,2′,4′,9′-tetrahydrospiro[piperidine-4,3′-pyrido[3,4-*b*]indole]-4′-carbonitrile (20**).** To a solution of **19** (270 mg, 0.58 mmol) in dichloromethane (30 mL) was added trifluoroacetic acid (7.5 mL), and the mixture was stirred at room temperature for 35 min. The volatile compounds were removed by azeotropic rotary evaporation with toluene (10 mL), and the residue was resuspended in 2 M NaOH solution (10 mL). After extraction with ethyl acetate (3 × 10 mL), the combined organic layers were dried over MgSO₄ and the solvent was evaporated. The crude product was recrystallized from ethanol to give 124 mg (59%) of **20** as white crystals. Mp 289 °C; ¹H NMR (500 MHz, DMSO-*d*₆) δ 8.32 (br s, 1 H, N–H), 7.91 (d, *J* = 8.5 Hz, 1 H, 5′-H), 7.44 (d, *J* = 8.5 Hz, 1 H, 6′-H), 5.08 (s, 1 H, 4′-H), 4.46 (s, 3 H, 9′-CH₃), 2.99 (m, 1 H, 2′-6′-H), 2.78 (m, 1 H, 2′-6′-H), 2.64 (m, 2 H, 2′-6′-H), 2.23 (br s, 1 H, 1-H), 1.89 (m, 2 H, 3′-5′-H), 1.59 (m, 2 H, 3′-5′-H); MS EI *m/z* (relative intensity, %) 366 [M⁺ + 4] (4), 364 [M⁺ + 2] (22), 362 [M⁺] (36), 317 (39), 305 (100), 236 (48), 195 (25). Anal. (C₁₇H₁₆Cl₂N₄O) C, H, N.

(4′RS)-7′,8′-Dichloro-1′-oxo-1′,2′,4′,9′-tetrahydrospiro[cyclohexane-1,3′-pyrido[3,4-*b*]indole]-4′-carbonitrile (22**).** **22** was prepared from **21**¹⁰ (1.00 g, 3.21 mmol) and cyclohexanone

(5 mL) following the general procedure for preparation of spiro 4-cyano-1-oxo- β -carbolines. Eluent for FCC was petroleum ether/ethyl acetate (1:1). The crude product was recrystallized from ethanol to give 220 mg (19%) of **22** as white crystals. Mp 281 °C; ¹H NMR (400 MHz, DMSO-*d*₆) δ 12.71 (br s, 1 H, 9'-H), 8.17 (br s, 1 H, 2'-H), 7.87 (d, *J* = 8.3 Hz, 1 H, 5'-H), 7.41 (d, *J* = 8.3 Hz, 1 H, 6'-H), 5.06 (s, 1 H, 4'-H), 1.95–1.35 (m, 10 H, 2-/3-/4-/5-/6-H); MS EI *m/z* (relative intensity, %) 351 [$M^{+} + 4$] (16), 349 [$M^{+} + 2$] (62), 347 [M^{+}] (100), 222 (34), 195 (43). Anal. (C₁₇H₁₅Cl₂N₃O) C, H, N.

(4'RS)-7',8'-Dichloro-9'-methyl-1'-oxo-1',2',4',9'-tetrahydrospiro[cyclohexane-1,3'-pyrido[3,4-*b*]indole]-4'-carbonitrile (9). Triethylbenzylammonium chloride (TEBAC; 200 mg, 0.877 mmol) and K₂CO₃ (138 mg, 1.00 mmol) were suspended in acetonitrile (30 mL), and the mixture was stirred for 15 min at room temperature. A solution of **22** (348 mg, 1.00 mmol) in acetonitrile (20 mL) was added, followed by slow addition of dimethyl sulfate (126 mg, 1.00 mmol), and the mixture was stirred at room temperature for 12 h. The solvent was removed by evaporation. The residue was redissolved in ethyl acetate (50 mL), and the mixture was washed with water (2 × 20 mL) and brine (2 × 20 mL). The aqueous layer was reextracted with ethyl acetate (20 mL). The combined organic layers were dried over MgSO₄, and the solvent was evaporated. The crude product was recrystallized from ethanol to give 202 mg (56%) of **9** as white crystals. Mp 290 °C. The spectral data were in full accordance with previously reported values.¹⁰ Anal. (C₁₈H₁₇Cl₂N₃O) C, H, N.

(4RS)-4-Aminomethyl-7,8-dichloro-3,3-dimethyl-2,3,4,9-tetrahydro-1H-pyrido[3,4-*b*]indol-1-one (23). Tetra-*N*-butylammonium borohydride (2.40 g, 9.31 mmol) and **5** (1.00 g, 3.10 mmol) were dissolved in dichloromethane (100 mL), and the mixture was refluxed for 24 h. After the mixture was cooled, the solvent was evaporated and the residue carefully resuspended in 2 M HCl solution (20 mL) followed by refluxing for 30 min. The mixture was poured onto ice, basified with 2 M NaOH, and extracted with ethyl acetate (3 × 10 mL). The combined organic layers were dried over MgSO₄, and the solvent was evaporated. The crude product was purified by FCC (eluent, dichloromethane/ethanol (5:1)). The product was recrystallized from toluene to give 400 mg (40%) of **23** as white needles. Mp 202 °C; ¹H NMR (400 MHz, CD₂Cl₂-*d*₂) δ 7.54 (d, *J* = 8.5 Hz, 1 H, 5-H), 7.21 (d, *J* = 8.5 Hz, 1 H, 6-H), 5.47 (br s, 1 H, 2-H), 4.53 (s, 3 H, N-CH₃), 3.08 (dd, *J* = 17.3 Hz, 8.0 Hz, 1 H, CH₂), 2.94 (dd, *J* = 17.3 Hz, 8.0 Hz, 1 H, CH₂), 2.93 (t, *J* = 8.0 Hz, 1 H, 4-H), 1.42 (s, 3 H, 3-CH₃), 1.29 (s, 3 H, 3-CH₃), 1.13 (s, 2 H, NH₂); MS EI *m/z* (relative intensity, %) 329 [$M^{+} + 4$] (1), 327 [$M^{+} + 2$] (4), 325 [M^{+}] (6), 296 (44), 281 (100). Anal. (C₁₅H₁₇Cl₂N₃O) C, H, N.

(4RS)-N-[(7,8-Dichloro-3,3-dimethyl-1-oxo-2,3,4,9-tetrahydro-1H-pyrido[3,4-*b*]indol-4-yl)methyl]acetamide (24). To a solution of **23** (388 mg, 1.19 mmol) in toluene (50 mL) was added acetic anhydride (123 mg, 1.20 mmol), and the mixture was stirred for 1 h at 80 °C. After the mixture was cooled, the solvent was removed by rotary evaporation and the residue purified by FCC. The eluent was dichloromethane/ethanol (5:1). Yield: 401 mg (91%) of **24** as white crystals. Mp 299 °C; ¹H NMR (400 MHz, DMSO-*d*₆) δ 7.74 (br t, *J* = 5.7 Hz, 2 H, N-H), 7.58 (d, *J* = 8.6 Hz, 1 H, 5-H), 7.32 (d, *J* = 8.6 Hz, 1 H, 6-H), 4.45 (s, 3 H, N-CH₃), 3.47 (ddd, *J* = 13 Hz, 7.0 Hz, 5.7 Hz, 1 H, CH₂), 3.12 (br t, *J* = 7.0 Hz, 1 H, 4-H), 2.97 (ddd, *J* = 13 Hz, 7.0 Hz, 5.7 Hz, 1 H, CH₂), 1.62 (s, 3 H, CO-CH₃), 1.34 (s, 3 H, 3-CH₃), 1.17 (s, 3 H, 3-CH₃); MS EI *m/z* (relative intensity, %) 371 [$M^{+} + 4$] (1), 369 [$M^{+} + 2$] (7), 367 [M^{+}] (11), 308 (64), 295 (100), 281 (38), 260 (33). Anal. (C₁₇H₁₉Cl₂N₃O₂) C, H, N.

Biochemical Assays. *Protein Purification.* PIM1 was purified as described previously.²⁰

DAPK3 (coding for residues V9 to G288) was cloned into the T7 expression vector pNIC28-Bsa4 and expressed as a TEV (tobacco etch virus protease) cleavable N-terminal His₆ fusion protein in the phage resistant strain BL21 (DE3) R3 co-transformed with a chloramphenicol resistant coexpression plasmid (pCOEX) expressing λ -phosphatase. An amount of 1 mL of an overnight culture was used to inoculate 2 L of TB medium containing 50 μ g/mL kanamycin and 40 μ g/mL chloramphenicol. *E. coli* cells were grown in 2.5 L baffled flasks at 37 °C until OD₆₀₀ reached 2.0. The cultures were cooled to 25 °C, and expression of DAPK3 was induced by adding 0.5 mM IPTG at an OD₆₀₀ of 2.2. Cells were

resuspended in lysis buffer (50 mM HEPES buffer, pH 7.5, 500 mM NaCl, 5% glycerol) and lysed by sonication. Nucleic acids and cell debris were removed by centrifugation. The cell lysate was loaded onto a Ni affinity, HisTrap, 5 mL column (GE/Amersham Biosciences) equilibrated in lysis buffer. The column was washed using 10 column volumes of 50 mM HEPES buffer, pH 7.5, 500 mM NaCl, 20 mM imidazole, and 5% glycerol, and DAPK3 was eluted using 50 mM HEPES buffer, pH 7.5, 500 mM NaCl, 150 mM imidazole, and 5% glycerol. DTT was added to a final concentration of 5 mM, and the His-tag was removed by the addition of 200 μ g of TEV protease (14 h at 4 °C). The protein was loaded onto a Hiload 16/60 Superdex 200 prep grade, 120 mL column (GE/Amersham Bioscience) equilibrated in 50 mM HEPES, pH 7.5, 500 mM NaCl, 5% glycerol, 5 mM DTT. After size exclusion chromatography the recombinant protein was more than 95% pure as judged by SDS-PAGE, and ESI-MS confirmed the correct mass of the protein. DAPK3 was concentrated to 12.6 mg/mL for crystallization studies.

Crystallization. Aliquots of the purified proteins were set up for crystallization using a mosquito crystallization robot (TTP Labtech, Royston U.K.). Coarse screens were typically set up onto Greiner three-well plates using three different drop ratios of precipitant to protein per condition (100 + 50 nL, 75 + 75 nL, and 50 + 100 nL). Initial hits were optimized further using Greiner three-well plates and scaling up the drop sizes in steps. Crystallizations were carried out using the sitting drop vapor diffusion method at 4 °C. PIM1 (6 mg/mL) was concentrated in the presence of 17 μ M β -carboline (17 or 20) and 17 μ M consensus peptide (ARKRRRHPSGPPTA-amide). Crystals with **17** were grown at 4 °C in 1.0 μ L sitting drops, mixing 0.75 μ L of the solution with 0.25 μ L of a reservoir solution containing 0.14 M sodium malonate, 0.07 M Bis-Tris propane, pH 7.5, 14% PEG 3350, 7% ethylene glycol. Crystals of PIM1 with **20** were grown at 4 °C in 1.0 μ L sitting drops, mixing 0.8 μ L of protein solution with 0.2 μ L of a reservoir solution containing 0.56 M sodium succinate, pH 7.0. Crystals of DAPK3 in complex with **20** were grown by mixing 50 μ L of the protein (12.6 mg/mL in the presence of 1 mM **20**) with 100 μ L of reservoir solution containing 0.1 M SPG, pH 6.0, 30.0% PEG 1K.

Data Collection and Structure Solution. Crystals were directly flash frozen in liquid nitrogen in the case of the DAPK3 complex or were supplemented by 20% ethylene glycol (in the case of the PIM1 complexes) and flash frozen. Data were collected on an FR-E Superbright source using an RAXIS IV plate detector at 1.542 Å (PIM1A/20) or at the Swiss Light Source beamline PX10 at 0.97912 Å (PIM1A/17) or 0.9807 Å (DAPK3/20). Indexing and integration were carried out using HKL-2000⁴² or MOSFLM,⁴³ and scaling was performed with SCALEPACK⁴² or SCALA.⁴⁴ Initial phases were calculated by molecular replacement with PHASER⁴⁵ using the known models of PIM1⁴¹ and DAP.⁴⁶ Initial models were built by ARP/wARP,⁴⁷ and building was completed manually with COOT.⁴⁸ Refinement was carried out in REFMAC5.⁴⁹ Thermal motions were analyzed using TLSMD,⁵⁰ and hydrogen atoms were included in late refinement cycles. Data collection and refinement statistics can be found in Table S2 (Supporting Information). The models and structure factors have been deposited with PDB accession codes 3CXW (PIM1/17), 3CY2 (PIM1/20), and 3BHY (DAPK3/17).

Cell Based Assays. *Cell Culture and Treatment with PIM Inhibitor.* Human leukemia cell lines MV4;11, RS4;11, MOLM13, SEM, and K562 were purchased from DSMZ and maintained in RPMI 1640 with 10% FCS and 1% penicillin/streptomycin at 37 °C in 5% CO₂. To evaluate the effect on the cell proliferation, **20** (0–10 μ M) was added to the culture medium and the cultures were incubated for 48 h. Cell proliferation and viability were assayed using cell proliferation reagent WST-1 from Roche Diagnostics according to the manufacturer's instructions. Cell survival was calculated as a percentage normalized to control cultures, and IC₅₀ values were calculated using GraphPad Prism.

Protein Extraction and Western Blotting. MV4;11 cells were grown at 5 × 10⁵/mL, treated with **20** at 0–10 μ M for various times, harvested, and rinsed with ice-cold PBS. Ice-cold lysis buffer [10 mM Tris-HCl (pH 7.4), 150 mM NaCl, 1% Triton X-100, 0.5 mM EDTA, 10% glycerol, 10 mM NaF, 1 mM Na₃VO₄, protease inhibitor cocktail] was added to the cells, and the mixture was incubated for 20 min on ice followed by 15 min of centrifugation at 12000g. Cleared lysates were assayed for protein concentration using the Bradford protein

assay system (Bio-Rad). An amount of 50 μg of protein was subjected to 15% SDS-PAGE and transferred onto a PVDF membrane. Membranes were blotted with primary antibodies (diluted according to the manufacturer's recommendations), followed by horseradish peroxidase-conjugated secondary antibodies, and the proteins were detected by SuperSignal West Femto maximum sensitivity substrate (Pierce). The same blots were stripped and reprobed with desired antibodies to confirm equal loading with the following antibodies: anti-phospho-4E-BP1, anti-4E-BP1 (Cell Signaling Technology), and anti- β -actin (Sigma).

■ ASSOCIATED CONTENT

Supporting Information

Thermal shift stability assay data, crystallographic data, interaction of **17** and **20** with PIM1, additional procedures and analytical data, and elemental analysis results. This material is available free of charge via the Internet at <http://pubs.acs.org>.

Accession Codes

[†]PDB codes for crystal structures of **17** and **20** in complex with PIM1 are 3CXW and 3CY2, respectively. PDB code for the cocrystal structure of **17** in complex with DAPK3 is 3BHY.

■ AUTHOR INFORMATION

Corresponding Author

*Phone: +49-89-2180 77301. Fax: +49-89-2180 77802. E-mail: franz.bracher@cup.uni-muenchen.de.

■ ACKNOWLEDGMENTS

We thank Monika Klimt for technical assistance. A.N.B., S.K., P.F., and O.F. are funded by the Structural Genomics Consortium, a registered charity (No. 1097737) that receives funds from the Canadian Institutes for Health Research, the Canadian Foundation for Innovation, Genome Canada through the Ontario Genomics Institute, GlaxoSmithKline, Karolinska Institutet, the Knut and Alice Wallenberg Foundation, the Ontario Innovation Trust, the Ontario Ministry for Research and Innovation, Merck & Co., Inc., the Novartis Research Foundation, the Swedish Agency for Innovation Systems, the Swedish Foundation for Strategic Research, and the Wellcome Trust.

■ ABBREVIATIONS USED

PIM, proviral integration site in Moloney murine leukemia virus; CK2, casein kinase II; RET, rearranged during transfection; TEBAC, triethylbenzylammonium chloride; CLK1, cdc2-like kinase 1; DAPK3, death-associated protein kinase 3; BMP2K, BMP2-inducible protein kinase; DRAK1, DAP-kinase-related apoptosis-inducing protein kinase 1

■ REFERENCES

- (1) Manning, G.; Whyte, D. B.; Martinez, R.; Hunter, T.; Sudarsanam, S. The Protein Kinase Complement of the Human Genome. *Science* **2002**, *298*, 1912–1934.
- (2) Buchdunger, E.; Zimmermann, J.; Mett, H.; Meyer, T.; Müller, M.; Druker, B. J.; Lydon, N. B. Inhibition of the Abl Protein-Tyrosine Kinase in Vitro and in Vivo by a 2-Phenylaminopyrimidine Derivative. *Cancer Res.* **1996**, *56*, 100–104.
- (3) Christensen, J. G.; Zou, H. Y.; Arango, M. E.; Li, Q.; Lee, J. H.; McDonnell, S. R.; Yamazaki, S.; Alton, G. R.; Mroczkowski, B.; Los, G. Cytoreductive antitumor activity of PF-2341066, a novel inhibitor of anaplastic lymphoma kinase and c-Met, in experimental models of anaplastic large-cell lymphoma. *Mol. Cancer Ther.* **2007**, *6*, 3314–3322.

- (4) Pohl, B.; Luchterhandt, T.; Bracher, F. Total Syntheses of the Chlorinated β -Carboline Alkaloids Bauerine A, B, and C. *Synth. Commun.* **2007**, *37*, 1273–1280.

- (5) Larsen, L. K.; Moore, R. E.; Patterson, G. M. Beta-Carbolines from the Blue-Green Alga *Dichothrix baueriana*. *J. Nat. Prod.* **1994**, *57*, 419–421.

- (6) Cincinelli, R.; Cassinelli, G.; Dallavalle, S.; Lanzi, C.; Merlini, L.; Botta, M.; Tuccinardi, T.; Martinelli, A.; Penco, S.; Zunino, F. Synthesis, Modeling, and RET Protein Kinase Inhibitory Activity of 3- and 4-Substituted β -Carboline-1-ones. *J. Med. Chem.* **2008**, *51*, 7777–7787.

- (7) Fedorov, O.; Huber, K.; Eisenreich, A.; Filippakopoulos, P.; King, O.; Bullock, A. N.; Szklarczyk, D.; Jensen, L. J.; Fabbro, D.; Trappe, J.; Rauch, U.; Bracher, F.; Knapp, S. Specific CLK Inhibitors from a Novel Chemotype for Regulation of Alternative Splicing. *Chem. Biol.* **2011**, *18*, 67–76.

- (8) Bissantz, C.; Kuhn, B.; Stahl, M. A Medicinal Chemist's Guide to Molecular Interactions. *J. Med. Chem.* **2010**, *53*, 5061–5084.

- (9) Battistutta, R.; Mazzorana, M.; Sarno, S.; Kazimierzczuk, Z.; Zanotti, G.; Pinna, L. A. Inspecting the Structure–Activity Relationship of Protein Kinase CK2 Inhibitors Derived from Tetrabromobenzimidazole. *Chem. Biol.* **2005**, *12*, 1211–1219.

- (10) Huber, K.; Kast, O.; Bracher, F. A Versatile Synthesis of 3-Substituted 4-Cyano-1,2,3,4-tetrahydro-1-oxo- β -carbolines. *Synthesis* **2010**, 3849–3854.

- (11) Brault, L.; Gasser, C.; Bracher, F.; Huber, K.; Knapp, S.; Schwaller, J. PIM Serine/Threonine Kinases in the Pathogenesis and Therapy of Hematologic Malignancies and Solid Cancers. *Haematologica* **2010**, *95*, 1004–1015.

- (12) Gozuacik, D.; Kimchi, A. DAPK Protein Family and Cancer. *Autophagy* **2006**, *2*, 74–79.

- (13) Mukhopadhyay, R.; Ray, P. S.; Arif, A.; Brady, A. K.; Kinter, M.; Fox, P. L. DAPK-ZIPK-L13a Axis Constitutes a Negative-Feedback Module Regulating Inflammatory Gene Expression. *Mol. Cell* **2008**, *32*, 371–382.

- (14) Haystead, T. A. J. ZIP Kinase, a Key Regulator of Myosin Protein Phosphatase 1. *Cell. Signalling* **2005**, *17*, 1313–1322.

- (15) Kocienski, P. J. *Protecting Groups*, 3rd ed.; Georg Thieme: Stuttgart, Germany, 2004.

- (16) Dubey, P. K.; Reddy, P. V. V. P. Unexpected Regiospecific Reduction of the Double Bond by NaBH_4 in 2-(1-Methyl/1H-benzimidazole-2-yl)-3-aryl-acrylonitrile. *Synth. Commun.* **2007**, *37*, 2259–2266.

- (17) Bracher, F. Polycyclische Aromatische Alkaloide, 10. Mitt.: Annonaceen-Alkaloide mit antimykotischer Aktivität. *Arch. Pharm.* **1994**, *327*, 371–375.

- (18) Satoh, T.; Suzuki, S.; Suzuki, Y.; Miyaji, Y.; Imai, Z. Reduction of Organic Compounds with Sodium Borohydride–Transition Metal Salt Systems: Reduction of Organic Nitrile, Nitro and Amide Compounds to Primary Amines. *Tetrahedron Lett.* **1969**, *10*, 4555–4558.

- (19) Wakamatsu, T.; Inaki, H.; Ogawa, A.; Watanabe, M.; Ban, Y. An Efficient Reduction of Nitriles and Amides to the Corresponding Amines with Tetra-*N*-butylammonium Borohydride in Dichloromethane. *Heterocycles* **1980**, *14*, 1437–1440.

- (20) Bullock, A. N.; Debreczeni, J. E.; Fedorov, O. Y.; Nelson, A.; Marsden, B. D.; Knapp, S. Structural Basis of Inhibitor Specificity of the Human Protooncogene Proviral Insertion Site in Moloney Murine Leukemia Virus (PIM-1) Kinase. *J. Med. Chem.* **2005**, *48*, 7604–7614.

- (21) Blanco-Aparicio, C.; Collazo, A. M. G.; Oyarzabal, J.; Leal, J. F.; Albarán, M. I.; Lima, F. R.; Pequeño, B.; Ajenjo, N.; Becerra, M.; Alfonso, P.; Reymundo, M. I.; Palacios, I.; Mateos, G.; Quiñones, H.; Corriero, A.; Carnero, A.; Pevarello, P.; Lopez, A. R.; Fominaya, J.; Pastor, J.; Bischoff, J. R. Pim 1 Kinase Inhibitor ETP-45299 Suppresses Cellular Proliferation and Synergizes with PI3K Inhibition. *Cancer Lett.* **2011**, *300*, 145–153.

- (22) Kim, M. K.; Min, J.; Choi, B.-Y.; Lim, H.; Cho, Y.-H.; Lee, C.-H. Discovery of Cyclin-Dependent Kinase Inhibitor, CR229, Using Structure-Based Drug Screening. *J. Microbiol. Biotechnol.* **2007**, *17*, 1712–1716.

- (23) Cheney, I. W.; Yan, S.; Appleby, T.; Walker, H.; Vo, T.; Yao, N.; Hamatake, R.; Hong, Z.; Wu, J. Z. Identification and Structure–Activity Relationships of Substituted Pyridones as Inhibitors of Pim-1 Kinase. *Bioorg. Med. Chem. Lett.* **2007**, *17*, 1679–1683.
- (24) Akué-Gédu, R.; Rossignol, E.; Azzaro, S. P.; Knapp, S.; Filippakopoulos, P.; Bullock, A. N.; Bain, J.; Cohen, P.; Prudhomme, M.; Anizon, F.; Moreau, P. Synthesis, Kinase Inhibitory Potencies, and in Vitro Antiproliferative Evaluation of New Pim Kinase Inhibitors. *J. Med. Chem.* **2009**, *52*, 6369–6381.
- (25) Tao, Z.-F.; Hasvold, L. A.; Levenson, J. D.; Han, E. K.; Guan, R.; Johnson, E. F.; Stoll, V. S.; Stewart, K. D.; Stamper, G.; Soni, N.; Bouska, J. J.; Luo, Y.; Sowin, T. J.; Lin, N.-H.; Giranda, V. S.; Rosenberg, S. H.; Penning, T. D. Discovery of 3*H*-Benzo[4,5]thieno-[3,2-*d*]pyrimidin-4-ones as Potent, Highly Selective, and Orally Bioavailable Inhibitors of the Human Protooncogene Proviral Insertion Site in Moloney Murine Leukemia Virus (PIM) Kinases. *J. Med. Chem.* **2009**, *52*, 6621–6636.
- (26) Holder, S.; Lilly, M.; Brown, M. L. Comparative Molecular Field Analysis of Flavonoid Inhibitors of the PIM-1 Kinase. *Bioorg. Med. Chem.* **2007**, *15*, 6463–6473.
- (27) Debreczeni, J. É.; Bullock, A. N.; Atilla, G. E.; Williams, D. S.; Bregman, H.; Knapp, S.; Meggers, E. Ruthenium Half-Sandwich Complexes Bound to Protein Kinase Pim-1. *Angew. Chem., Int. Ed.* **2006**, *45*, 1580–1585.
- (28) Qian, K. C.; Wang, L.; Hickey, E. R.; Studts, J.; Barringer, K.; Peng, C.; Kronkaitis, A.; Li, J.; White, A.; Mische, S.; Farmer, B. Structural Basis of Constitutive Activity and a Unique Nucleotide Binding Mode of Human Pim-1 Kinase. *J. Biol. Chem.* **2005**, *280*, 6130–6137.
- (29) Qian, K.; Wang, L.; Cywin, C. L.; Farmer, B. T.; Hickey, E.; Homon, C.; Jakes, S.; Kashem, M. A.; Lee, G.; Leonard, S.; Li, J.; Magboo, R.; Mao, W.; Pack, E.; Peng, C.; Prokopowicz, A.; Welzel, M.; Wolak, J.; Morwick, T. Hit to Lead Account of the Discovery of a New Class of Inhibitors of Pim Kinases and Crystallographic Studies Revealing an Unusual Kinase Binding Mode. *J. Med. Chem.* **2009**, *52*, 1814–1827.
- (30) Bullock, A. N.; Russo, S.; Amos, A.; Pagano, N.; Bregman, H.; Debreczeni, J. É.; Lee, W. H.; Delft, F. v.; Meggers, E.; Knapp, S. Crystal Structure of the PIM2 Kinase in Complex with an Organoruthenium Inhibitor. *PLoS One* **2009**, *4*, e7112.
- (31) Bullock, A. N.; Debreczeni, J.; Amos, A. L.; Knapp, S.; Turk, B. E. Structure and Substrate Specificity of the Pim-1 Kinase. *J. Biol. Chem.* **2005**, *280*, 41675–41682.
- (32) Amson, R.; Sigaux, F.; Przedborski, S.; Flandrin, G.; Givol, D.; Telerman, A. The Human Protooncogene Product p33pim Is Expressed during Fetal Hematopoiesis and in Diverse Leukemias. *Proc. Natl. Acad. Sci. U.S.A.* **1989**, *86*, 8857–8861.
- (33) Cohen, A. M.; Grinblat, B.; Bessler, H.; Kristt, D. A.; Kremer, A.; Shalom, S.; Schwartz, A.; Halperin, M.; Merkel, D.; Don, J. Increased Expression of the *hPim-2* Gene in Human Chronic Lymphocytic Leukemia and Non-Hodgkin Lymphoma. *Leuk. Lymphoma* **2004**, *45*, 951–955.
- (34) Kim, K.-T.; Baird, K.; Ahn, J.-Y.; Meltzer, P.; Lilly, M.; Levis, M.; Small, D. Pim-1 Is up-Regulated by Constitutively Activated FLT3 and Plays a Role in FLT3-Mediated Cell Survival. *Blood* **2005**, *105*, 1759–1767.
- (35) Pasqualucci, L.; Neumeister, P.; Goossens, T.; Nanjangud, G.; Chaganti, R. S. K.; Kuppers, R.; Dalla-Favera, R. Hypermutation of Multiple Proto-Oncogenes in B-Cell Diffuse Large-Cell Lymphomas. *Nature* **2001**, *412*, 341–346.
- (36) Schatz, J. H.; Oricchio, E.; Wolfe, A. L.; Jiang, M.; Linkov, I.; Maragulia, J.; Shi, W.; Zhang, Z.; Rajasekhar, V. K.; Pagano, N. C.; Porco, J. A.; Teruya-Feldstein, J.; Rosen, N.; Zelenetz, A. D.; Pelletier, J.; Wendel, H.-G. Targeting Cap-Dependent Translation Blocks Converging Survival Signals by AKT and PIM Kinases in Lymphoma. *J. Exp. Med.* **2011**, *208*, 1799–1807.
- (37) Valdman, A.; Fang, X.; Pang, S.-T.; Ekman, P.; Egevad, L. Pim-1 Expression in Prostatic Intraepithelial Neoplasia and Human Prostate Cancer. *Prostate* **2004**, *60*, 367–371.
- (38) Wang, J.; Kim, J.; Roh, M.; Franco, O. E.; Hayward, S. W.; Wills, M. L.; Abdulkadir, S. A. Pim1 Kinase Synergizes with c-MYC To Induce Advanced Prostate Carcinoma. *Oncogene* **2010**, *29*, 2477–2487.
- (39) Popivanova, B. K.; Li, Y. Y.; Zheng, H.; Omura, K.; Fujii, C.; Tsuneyama, K.; Mukaida, N. Proto-Oncogene, Pim-3 with Serine/Threonine Kinase Activity, Is Aberrantly Expressed in Human Colon Cancer Cells and Can Prevent Bad-Mediated Apoptosis. *Cancer Sci.* **2007**, *98*, 321–328.
- (40) Li, Y.-Y.; Popivanova, B. K.; Nagai, Y.; Ishikura, H.; Fujii, C.; Mukaida, N. Pim-3, a Proto-Oncogene with Serine/Threonine Kinase Activity, Is Aberrantly Expressed in Human Pancreatic Cancer and Phosphorylates Bad to Block Bad-Mediated Apoptosis in Human Pancreatic Cancer Cell Lines. *Cancer Res.* **2006**, *66*, 6741–6747.
- (41) Pogacic, V.; Bullock, A. N.; Fedorov, O.; Filippakopoulos, P.; Gasser, C.; Biondi, A.; Meyer-Monard, S.; Knapp, S.; Schwaller, J. Structural Analysis Identifies Imidazo[1,2-*b*]Pyridazines as PIM Kinase Inhibitors with in vitro Antileukemic Activity. *Cancer Res.* **2007**, *67*, 6916–6924.
- (42) Otwinowski, Z.; Minor, W. Processing of X-ray Diffraction Data Collected in Oscillation Mode. In *Macromolecular Crystallography. Part A*; Carter, C. W., Jr., Sweet, R. M., Eds.; Academic Press: San Diego, CA, 1997; Vol. 276, pp 307–326.
- (43) Leslie, A. G. W.; Powell, H. *MOSFLM*, version 7.01; MRC Laboratory of Molecular Biology: Cambridge, U.K., 2007.
- (44) Evans, P. *SCALA: Scale Together Multiple Observations of Reflections*, version 3.3.0; MRC Laboratory of Molecular Biology: Cambridge, U.K., 2007.
- (45) McCoy, A. J.; Grosse-Kunstleve, R. W.; Storoni, L. C.; Read, R. J. Likelihood-Enhanced Fast Translation Functions. *Acta Crystallogr., Sect. D: Biol. Crystallogr.* **2005**, *61*, 458–464.
- (46) de Diego, I.; Kuper, J.; Bakalova, N.; Kursula, P.; Wilmanns, M. Molecular Basis of the Death-Associated Protein Kinase–Calcium/Calmodulin Regulator Complex. *Sci. Signaling* **2010**, *3*, ra6.
- (47) Perrakis, A.; Morris, R.; Lamzin, V. S. Automated Protein Model Building Combined with Iterative Structure Refinement. *Nat. Struct. Biol.* **1999**, *6*, 458–463.
- (48) Emsley, P.; Cowtan, K. Coot: Model-Building Tools for Molecular Graphics. *Acta Crystallogr., Sect. D: Biol. Crystallogr.* **2004**, *60*, 2126–2132.
- (49) Murshudov, G. N.; Vagin, A. A.; Dodson, E. J. Refinement of Macromolecular Structures by the Maximum-Likelihood Method. *Acta Crystallogr., Sect. D: Biol. Crystallogr.* **1997**, *53*, 240–255.
- (50) Painter, J.; Merritt, E. A. Optimal Description of a Protein Structure in Terms of Multiple Groups Undergoing TLS Motion. *Acta Crystallogr., Sect. D: Biol. Crystallogr.* **2006**, *62*, 439–450.